Cell

# $Ca_V1$ and $Ca_V2$ Channels Engage Distinct Modes of $Ca^{2+}$ Signaling to Control CREB-Dependent Gene Expression

Damian G. Wheeler,[1,3,4] Rachel D. Groth,[1,3,5] Huan Ma,[1,2,3,*] Curtis F. Barrett,[1,6] Scott F. Owen,[1] Parsa Safa,[1] and Richard W. Tsien[1,2,*]

[1]Department of Molecular and Cellular Physiology, Stanford University School of Medicine, Stanford, CA 94305-5345, USA
[2]NYU Neuroscience Institute, NYU Langone Medical Center, New York, NY 10016, USA
[3]These authors contributed equally to this work
[4]Present address: Dart NeuroScience LLC, 7473 Lusk Boulevard, San Diego, CA 92121, USA
[5]Present address: Centers for Therapeutic Innovation, Pfizer Inc., 1700 Owens Street, San Francisco, CA 94158, USA
[6]Present address: English Editing Solutions, Oegstgeest 2343KW, The Netherlands
*Correspondence: huan.ma@nyumc.org (H.M.), richard.tsien@nyumc.org (R.W.T.)
DOI 10.1016/j.cell.2012.03.041

## SUMMARY

Activity-dependent gene expression triggered by $Ca^{2+}$ entry into neurons is critical for learning and memory, but whether specific sources of $Ca^{2+}$ act distinctly or merely supply $Ca^{2+}$ to a common pool remains uncertain. Here, we report that both signaling modes coexist and pertain to $Ca_V1$ and $Ca_V2$ channels, respectively, coupling membrane depolarization to CREB phosphorylation and gene expression. $Ca_V1$ channels are advantaged in their voltage-dependent gating and use nanodomain $Ca^{2+}$ to drive local CaMKII aggregation and trigger communication with the nucleus. In contrast, $Ca_V2$ channels must elevate $[Ca^{2+}]_i$ microns away and promote CaMKII aggregation at $Ca_V1$ channels. Consequently, $Ca_V2$ channels are ~10-fold less effective in signaling to the nucleus than are $Ca_V1$ channels for the same bulk $[Ca^{2+}]_i$ increase. Furthermore, $Ca_V2$-mediated $Ca^{2+}$ rises are preferentially curbed by uptake into the endoplasmic reticulum and mitochondria. This source-biased buffering limits the spatial spread of $Ca^{2+}$, further attenuating $Ca_V2$-mediated gene expression.

## INTRODUCTION

A central issue in calcium signaling is how cells use $Ca^{2+}$ delivered via multiple routes to trigger responses. A classic view is that multiple $Ca^{2+}$ sources contribute convergently to the bulk cytoplasmic $Ca^{2+}$ pool. An alternative view is that individual $Ca^{2+}$ delivery systems may trigger specific cellular effects by using "private lines" of communication. Multiple $Ca^{2+}$ sources contribute to a common $Ca^{2+}$ pool in the context of smooth muscle excitation-contraction (E-C) coupling (Berridge, 2008): $Ca_V1$ (L-type) $Ca^{2+}$ channels, surface pumps and exchangers, and sarcoplasmic reticulum each influence bulk $[Ca^{2+}]_i$ and, in turn, calmodulin molecules throughout the myoplasm. In contrast, neuronal excitation-secretion (E-S) coupling employs local signaling between $Ca_V2$ (N-, P/Q-, and R-type) $Ca^{2+}$ channels and, only nanometers away, the $Ca^{2+}$ sensor synaptotagmin, which triggers exocytosis (Sudhof, 2004).

Excitation-transcription (E-T) coupling, less understood than E-C or E-S coupling, provides a fresh opportunity to explore operating principles linking multiple $Ca^{2+}$ sources and cellular responses. The control of transcription is critically important for long-term adaptive changes during neuronal development, learning and memory, and drug addiction. It has long been recognized that $Ca_V1$ channels engage $Ca^{2+}$-dependent signal transduction pathways that alter transcription (Greenberg et al., 1986; Morgan and Curran, 1986; Murphy et al., 1991). Much is known about the workings of multiple channel types that control $Ca^{2+}$ entry in response to neuronal activity (Catterall, 2000; Dolphin, 2006; Tsien et al., 1991) and the diverse signal transduction pathways that drive transcription factor activation in response to $Ca^{2+}$ elevation (Deisseroth et al., 2003; Flavell and Greenberg, 2008). However, the organization of signaling between $Ca^{2+}$ entry and regulation of gene expression is still a matter of debate. One long-standing mystery is how $Ca_V1$ channels contribute only a minority of the overall $Ca^{2+}$ entry yet exert such a dominant role in controlling gene expression. A partial answer was provided by evidence that $Ca_V1$ channels can signal through $Ca^{2+}$ acting on local signaling machinery (Deisseroth et al., 1996; Dolmetsch et al., 2001; Oliveria et al., 2007; Weick et al., 2003; Wheeler et al., 2008). However, under certain conditions, $Ca_V2$ channels also trigger gene expression (Brosenitsch and Katz, 2001; Sutton et al., 1999; Zhao et al., 2007), and rises in bulk cytosolic or nuclear $Ca^{2+}$ also contribute (Adams and Dudek, 2005; Hardingham et al., 1997, 2001; Saha and Dudek, 2008). $Ca_V2$ channels make up the majority of somatodendritic $Ca^{2+}$ channels (Kavalali et al., 1997; Randall and Tsien, 1995; Regan et al., 1991) but appear less important than $Ca_V1$ in signaling to the nucleus. Is this a matter of uneven activation of the various channel types (Kasai and Neher, 1992;

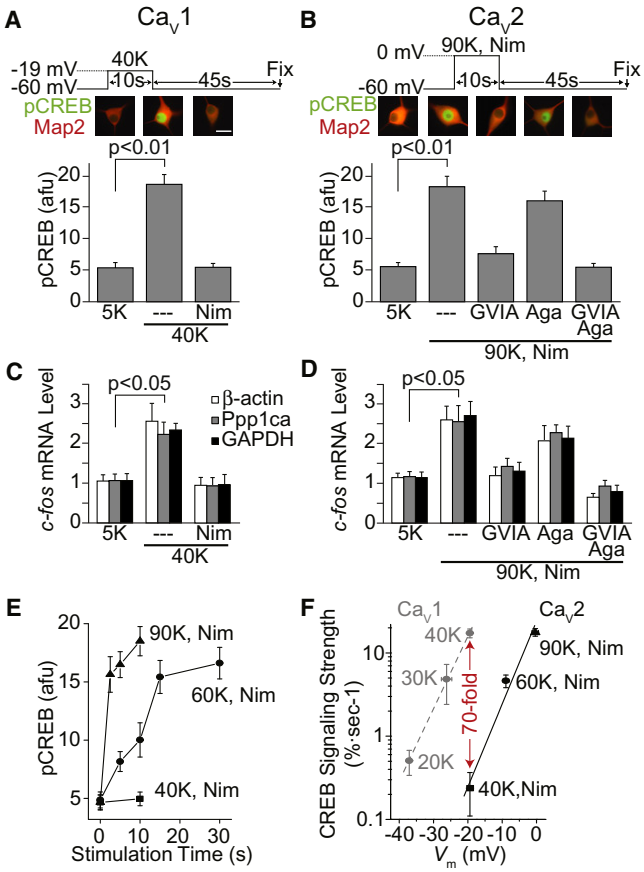


**Figure 1. Mild Depolarization Signals Exclusively through Ca$_V$1 Channels, whereas Stronger Depolarization Recruits Ca$_V$2 Channels**

(A) CREB phosphorylation evoked by 40K depolarization to −19mV was blocked by the Ca$_V$1 channel blocker Nim (10 μM). Scale bar, 30 μm.

(B) CREB phosphorylation resulting from 90K, Nim ± Ca$_V$2.2 toxin GVIA (2 μM), and Ca$_V$2.1 toxin Aga (500 nM). Data from ≥30 cells per condition from two platings.

(C and D) Neurons stimulated for 3 min and then placed in 5K Tyrode's for 42 min before RNA extraction and quantitative RT-PCR for *c-fos*. Data normalized against three housekeeping genes, plotted relative to control. n = 9 coverslips from three platings.

(E) pCREB levels for various durations of depolarization (≥50 cells, four platings).

(F) CREB signal strength extracted as initial slope of the plots in (E), plotted against measured membrane potentials (n ≥ 5). Fitted line shows steeply rising Ca$_V$2 signaling (*e*-fold change per 4.37mV). Gray, steepness of Ca$_V$1 channel signaling (Wheeler et al., 2008).

Error bars represent SEM.

Liu et al., 2003), or is $Ca^{2+}$ entry via Ca$_V$2 channels inherently less effective? If the latter is the case, are there mechanisms that amplify or attenuate the impact of specific routes of $Ca^{2+}$ entry?

We systematically compared the impact of various $Ca^{2+}$ channels in supporting $Ca^{2+}$ entry, bulk $[Ca^{2+}]_i$ rises, and changes in cAMP response element-binding protein (CREB) phosphorylation and gene expression. The efficacy of signaling via Ca$_V$1 and Ca$_V$2 channels differs markedly for a given depolarization and even for the same rise in bulk $[Ca^{2+}]_i$. Unlike Ca$_V$1 channels, Ca$_V$2 channels use a fundamentally different mode of $Ca^{2+}$ signaling that requires spread of the $Ca^{2+}$ signal over longer distances. Further, we reveal that the endoplasmic reticulum (ER) and mitochondria selectively buffer $Ca^{2+}$ entering through Ca$_V$2 channels and thereby restrict the impact of Ca$_V$2 channels on transcription.

## RESULTS

### Signaling to the Nucleus via Ca$_V$1 and Ca$_V$2 Is Differentially Encoded by Stimulus Intensity

Among the various voltage-gated $Ca^{2+}$ channels (VGCCs), Ca$_V$1 channels couple membrane depolarization to nuclear transcription (Greenberg et al., 1986; Morgan and Curran, 1986; Murphy et al., 1991), but the role for Ca$_V$2 channels is less clear. To determine their contribution to CREB phosphorylation in the nucleus, we K-depolarized cultured superior cervical ganglion (SCG) neurons in the presence of channel-specific blockers. Depolarizing to −19mV led to Ca$_V$1-channel-dependent serine133 CREB phosphorylation (Figure 1A) (Wheeler et al., 2006, 2008). Blocking Ca$_V$2 channels had no effect on this pCREB response (Figure S1A available online). In contrast, CREB phosphorylation appeared to depend on Cav2 channels when cells were depolarized to ~0mV. In this case, blocking Ca$_V$1 channels did not prevent CREB phosphorylation (Figures 1B and S1A), and the remaining non-Ca$_V$1 signaling was completely prevented by Ca$_V$2 channel blockade (Figure 1B).

Using qPCR for a CREB reporter gene (*hCMV-EGFP*; Wheeler and Cooper, 2001) and for two endogenous CREB target genes, *BDNF* (Shieh et al., 1998; Tao et al., 1998) and *c-fos* (Sheng et al., 1990), we found that prolonged depolarization to −19mV (0.75–3 hr) produced a robust Ca$_V$1 channel-dependent increase in *EGFP*, *BDNF*, and *c-fos* mRNA (Figures S1B–1D). To mimic our pCREB experiments more closely, we similarly depolarized neurons but for only 3 min. This brief stimulation led to an ~2.5-fold, Ca$_V$1-dependent increase in *c-fos* levels 45 min later (Figure 1C), resembling Ca$_V$1-dependent signaling to CREB (Figure 1A). Depolarization to ~0mV while blocking Ca$_V$1 channels increased *c-fos* expression via recruitment of Ca$_V$2.1 and Ca$_V$2.2 channels (Figure 1D), further paralleling the pCREB response (Figure 1B).

The effectiveness of excitation-response coupling depends on how signaling increases with depolarization level. Ca$_V$1-mediated signaling is steeply voltage dependent, changing *e*-fold (=2.73-fold) per ~5mV (Wheeler et al., 2008). For Ca$_V$2 signaling, we graphed the degree of CREB phosphorylation against the duration of various depolarizations in the presence of the Ca$_V$1 blocker, nimodipine (Nim) (Figure 1E). The signal strength, gauged by the initial slope of the rise in pCREB (see Experimental Procedures and Wheeler et al., 2008), increased *e*-fold per 4.37mV (Figure 1F). This relationship was just as steep as that for Ca$_V$1 channels but was displaced to more depolarized potentials so that signal strength was ~70-fold smaller at −20mV. Thus, with mild depolarizations, Ca$_V$1 channels dominate signaling to CREB (Figures 1F and S1A), whereas stronger depolarizations bring out involvement of Ca$_V$2 channels (Figure 1B).

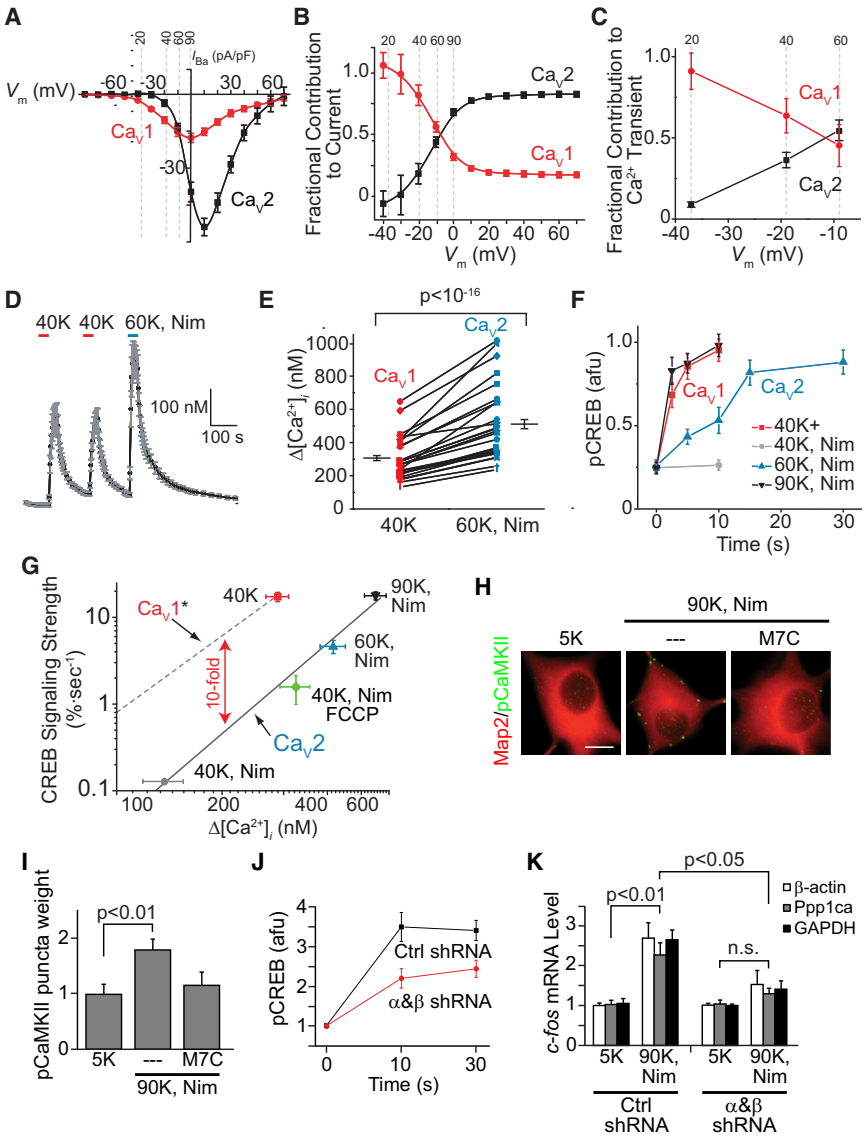


**Figure 2. $Ca_V1$ Channels Are Advantaged over $Ca_V2$ Channels in Signaling to CREB via CaMKII**

(A) Current-voltage relationships of $Ca_V1$ and $Ca_V2$ channels. Difference between total current and current in GVIA+Aga taken as $Ca_V2$ mediated. The remainder was considered $Ca_V1$ mediated. n = 3. Voltages produced by 20K–90K are indicated.

(B) Fractional contribution of $Ca_V1$ and $Ca_V2$ channels derived from tail currents (see Figure S1F).

(C) $Ca_V1$- and $Ca_V2$-based portions of $Ca^{2+}$ transient, obtained with K depolarizations ±Nim. Nim-sensitive portion deemed $Ca_V1$; remainder designated as $Ca_V2$ (n = 18 neurons).

(D) Fura-2 $Ca^{2+}$ signals from 5 DIV SCG neurons depolarized with 40 or 60K, Nim for 30 s. 40K was chosen so that the largely $Ca_V1$-mediated $\Delta[Ca^{2+}]_i$ was smaller than $Ca_V2$-mediated $\Delta[Ca^{2+}]_i$. Pooled data from four neurons in one field.

(E) The $Ca^{2+}$ transient was invariably larger with 60K, Nim (blue), than with 40K (red) ($p < 10^{-16}$). Lines connect data from the same cell, six experiments performed on one culture. Black bars, pooled data from multiple cultures (53 cells total).

(F) pCREB levels, normalized to 40K, 3 min response, plotted against time. For reference, the 40 and 90K with Nim data, normalized, are replicated from Figure 1E. >60 neurons, three to four experiments.

(G) CREB signal strength, obtained from (F), plotted against the corresponding peak $[Ca^{2+}]_i$ transient. Fura-2 $Ca^{2+}$ signals from 25–42 cells from 2–4 independent cultures. The data for 40, 60, and 90K with Nim were fit by a straight line, slope 3.46 (R = 0.997). The dashed line going through the 40K point has a slope reflecting the $[Ca^{2+}]$ dependence of $Ca_V1$ signaling previously determined (Wheeler et al., 2008). Green symbol is based on data in Figures 4G and 5E.

(H) Neurons stimulated with 90K + Nim for 10 s, immediately fixed and then stained for Map2 (red) and pCaMKII (green). Background pCaMKII staining was subtracted (Experimental Procedures). Scale bar, 10 μm.

(I) pCaMKII puncta weight from experiments as in (H). n = 3 independent experiments.

(J) SCG neurons infected with lentivirus expressing α and βCaMKII shRNA or control lentivirus were stimulated with 90K, Nim for the indicated durations, and stained for pCREB.

(K) *c-fos* mRNA in SCG neurons infected as in (J) and stimulated with 90K, Nim for 180 s, followed by 42 min in 5K to allow time for transcription. n = 3–4 experiments done in triplicate.

Error bars represent SEM.

## $Ca_V1$ Channels Have a "Gating Advantage" over $Ca_V2$ Channels

To clarify the $Ca_V1$ channel advantage in signaling to CREB, we recorded $Ca_V1$ and $Ca_V2$ channel currents in cultured SCG neurons. We found no evidence for $Ca_V3$ (T-type) (data not shown) or $Ca_V2.3$ (R-type) channel expression (Figure S1E). In combination, $Ca_V2.1$ and $Ca_V2.2$ blockers eliminated all $Ca_V2$ currents (~65%); the remaining current was blocked by the $Ca_V1$ inhibitor, Nim. Thus, $Ca_V1$ channels support only a minority of the total $Ca_V$ current, despite their advantage in signaling to CREB. We measured the degree of channel activation at various voltages by analyzing tail currents. $Ca_V2$ channels became activated at more positive potentials than $Ca_V1$channels, requiring ~17mV more depolarization for 50% activation (Figure S1F). This gating voltage advantage for $Ca_V1$ channels must be weighed against their smaller maximal flux, reflected by the respective current-voltage relationships (Figure 2A). The fractional contribution of $Ca_V1$ channels predominated at more negative potentials, attained with 20K (20 mM $K^+$; −37mV) or 40K (−19mV); and $Ca_V2$ channels caught up with 60K (−9mV) and predominated with even greater depolarization (Figure 2B). To verify that the balance tipped in the same way during

sustained depolarizations, we turned to Fura-2 ratiometric $Ca^{2+}$ imaging. Consistently, $Ca_V1$ channels contributed the majority of the $Ca^{2+}$ transient induced by 20K and 40K depolarizations and only ~50% with a stronger 60K depolarization (Figure 2C). Thus, voltage dependence puts $Ca_V1$ channels at a relative, though not absolute, advantage that is outweighed by the $Ca_V2$ current beyond a restricted voltage range.

## Differing Efficacy of $Ca^{2+}$ Entering through $Ca_V1$ versus $Ca_V2$ Channels

To find out whether $Ca_V1$ channels enjoy advantages beyond their ability to activate at more negative voltages, we related CREB signal strength to elevations in bulk $[Ca^{2+}]_i$ accompanying selectively activated signaling by the respective channel types. Strikingly, *smaller* $[Ca^{2+}]_i$ elevation was associated with *stronger* CREB signaling when $Ca_V1$-mediated signaling was compared with $Ca_V2$-mediated signaling (Figures 2D–2G). Whereas the $Ca_V2$-mediated $Ca^{2+}$ transient was consistently larger than that resulting from 40K (Figure 2E), $Ca_V2$ channels signaled less effectively (Figure 2F, blue) than $Ca_V1$ channels (Figure 2F, red). Only when $Ca_V2$ channels were activated by much stronger stimuli (Figure 2F, black) did their signaling strength reach that attained by $Ca_V1$ channels.

This finding is further highlighted by plotting signal strength as a function of bulk $[Ca^{2+}]_i$ elevation (Figure 2G), bypassing differences in channel voltage dependence described previously. $Ca_V2$-dependent signaling was a steep function of the $Ca^{2+}$ transient magnitude that follows a power law with $n = 3.46 \pm 0.26$ (Figure 2G), matching the steepness of $Ca_V1$-mediated signaling (dashed line, Figure 2G; derived from Wheeler et al. [2008], $p > 0.3$, generalized linear model [GLM]-analysis of covariance [ANCOVA]). Importantly, $Ca_V1$ and $Ca_V2$ channels do not obey a single relationship with the bulk $[Ca^{2+}]_i$ rise. Instead, $Ca^{2+}$ elevations resulting from $Ca_V1$ channels appeared ~10 times more efficient than $Ca^{2+}$ emanating from $Ca_V2$ channels (Figure 2G).

## Do $Ca_V1$ and $Ca_V2$ Channels Recruit Different Biochemical Cascades?

These source-specific differences in $Ca^{2+}$ signaling efficiency suggest a critical difference in cell signaling mechanisms downstream of $Ca^{2+}$ influx. To our surprise, pharmacological tests showed that the two channel classes employ similar signal transduction pathways (Figures S2A–2C). Like $Ca_V1$ signaling (Wheeler et al., 2008), rapid $Ca_V2$ signaling to CREB appeared to be mediated by a calmodulin (CaM) kinase-dependent pathway without any obvious requirement for activation of protein kinase A (PKA), protein kinase C (PKC), or mitogen-activated protein kinase (MAPK). This led us to ask whether CaMKII links $Ca_V2$ signaling to CREB, as it does for $Ca_V1$ channels. To quantify the extent of CaMKII activation, we identified pCaMKII puncta by an automated criterion (see Experimental Procedures) and found that $Ca_V2$ channel activation increased CaMKII phosphorylation within 10 s (Figures 2H and 2I).

To test for a causal role for CaMKII in $Ca_V2$-mediated signaling to CREB, we knocked down the major CaMKII subunits. Reducing mRNA for α- and β-CaMKII by 75% and 90%, respectively (Figures S2D and S2E), impaired the ability of $Ca_V2$ channels to signal to CREB (Figure 2J) and to induce *c-fos* (Figure 2K), just as previously found for $Ca_V1$. Evidently, the disparate $[Ca^{2+}]_i$ dependence of signaling to CREB (Figure 2G) cannot be attributed to utilization of different biochemical pathways by $Ca_V1$ or $Ca_V2$ channels.

## $Ca_V1$ Channels Signal to CREB via Local $Ca^{2+}$, whereas $Ca^{2+}$ Entering through $Ca_V2$ Channels Acts More Distantly

As an alternative, differences in signaling potency might stem from differences in spatial aspects of $Ca^{2+}$ signaling. Whereas $Ca_V1$ channels initiate signaling to the nucleus through $Ca^{2+}$ action on local signaling machinery (Deisseroth et al., 1996; Dolmetsch et al., 2001; Oliveria et al., 2007; Weick et al., 2003; Wheeler et al., 2008), $Ca^{2+}$ delivered by $Ca_V2$ channels might act at a greater distance. To test this hypothesis, we used $Ca^{2+}$ chelators: BAPTA suppresses rises in $Ca^{2+}$ very near the channel pore, whereas EGTA has a 100-fold slower on rate and thus allows a larger plume of elevated $Ca^{2+}$ in a nanodomain near the channel while suppressing rises in bulk $Ca^{2+}$ microns away. We evoked $Ca_V1$- and $Ca_V2$-dependent signaling in neurons pre-exposed to EGTA-AM, BAPTA-AM, or control solutions. Incorporation of BAPTA, but not EGTA, completely blocked $Ca_V1$-mediated signaling to CREB (Figures 3A and S3A). In contrast, both EGTA and BAPTA fully inhibited signaling through $Ca_V2$ channels (Figure 3A). These findings confirm that, unlike $Ca_V1$ channels, $Ca^{2+}$ entering through $Ca_V2$ channels must act far enough away from the source to be intercepted by EGTA.

## Accumulation of CaMKII near $Ca_V1$ Channels, but Not $Ca_V2$ Channels

How can $Ca_V1$ and $Ca_V2$ channels both utilize CaMKII to signal to CREB, whereas only $Ca_V1$ channels signal locally? Pre-existing tethering of CaMKII to $Ca_V1$ channels (Grueter et al., 2006; Hudmon et al., 2005; Wheeler et al., 2008) does not suffice as an explanation, as CaMKII also interacts with $Ca_V2$ channels (Jiang et al., 2008). However, $Ca_V1$ channels might be better able to recruit *diffusible* CaMKII molecules. Depolarization produces phospho-CaMKII puncta at the cell surface (Wheeler et al., 2008). These puncta colocalize with newly formed clusters of βCaMKII, the predominant CaMKII isoform in SCG neurons (Figures 3B and S3C), indicating a frank aggregation of CaMKII. Notably, $Ca_V1$-mediated formation of βCaMKII puncta was blocked by BAPTA, but not EGTA, at −19mV, whereas both chelators prevented $Ca_V2$-mediated formation of βCaMKII puncta at ~0mV (Figure 3C). Thus, the disparity between $Ca_V1$ and $Ca_V2$ extends to the spatial aspects of signaling to βCaMKII clusters.

We found that $Ca_V1.3$ immunoreactivity was partially punctate and generally coincident with the βCaMKII puncta (Figure 3D). After 40K depolarization, the separation between a βCaMKII punctum and the closest $Ca_V1.3$ channel cluster averaged $0.16 \pm 0.02$ μm (Figure 3F). For $Ca_V2$ channels, we used antibodies directed against $Ca_V2.1$ (see Supplemental Information). $Ca_V2.1$ immunoreactivity was highly punctate, but not coincident, with the activity-dependent βCaMKII clusters (Figure 3E). The separation between βCaMKII puncta and the

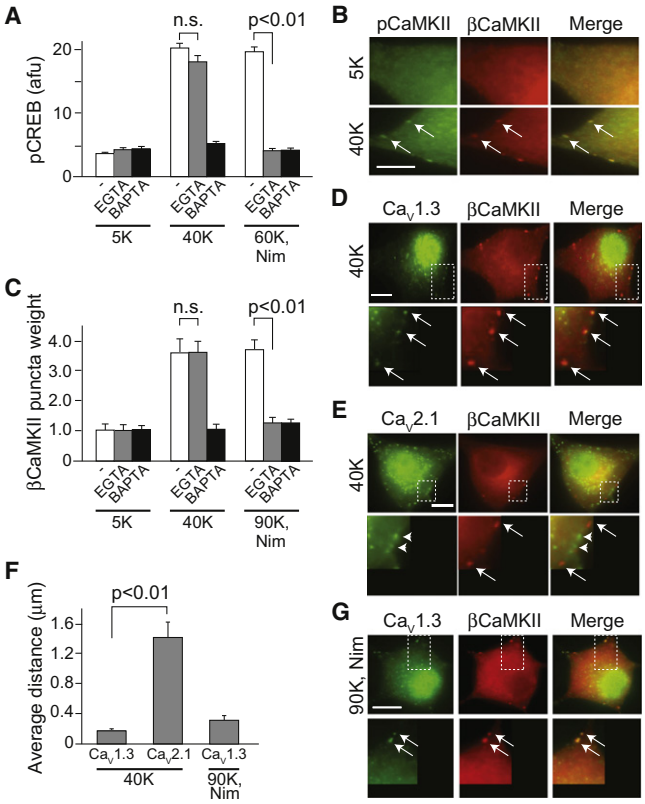


**Figure 3. $Ca^{2+}$ through $Ca_V1$ Channels Engages Signaling Locally, whereas $Ca_V2$-Derived $Ca^{2+}$ Acts at a Distance from the Channel**

(A) Neurons, mock loaded (–) or loaded with 100 μM EGTA-AM or BAPTA-AM, were stimulated for 60 s with 40 or 60K with Nim to activate $Ca_V1$- and $Ca_V2$-dependent signaling to CREB, respectively, and were then incubated for 45 s in 5K solution before fixation and staining for pCREB. n ≥ 50 neurons per condition, three separate cultures.

(B) Representative images of neurons stimulated with 40K for 10 s and stained for pCaMKII (green) and βCaMKII (red). Scale bar, 5 μm. pCaMKII puncta colocalized with βCaMKII puncta (arrows).

(C) Neurons loaded with EGTA or BAPTA were stimulated for 60 s as in (A), fixed immediately after stimulation, and stained for βCaMKII. Data are from ≥30 cells per condition from three platings.

(D) Neurons stimulated with 40K and stained with antibodies against $Ca_V1.3$ and βCaMKII. Arrows, sites where βCaMKII puncta colocalize with $Ca_V1.3$ channels.

(E) Neurons stimulated with 40K and stained with antibodies against $Ca_V2.1$ and βCaMKII. βCaMKII puncta (arrows) are located at sites distinct from $Ca_V2.1$ channel puncta (arrowheads).

(F) Average nearest-neighbor distance from βCaMKII puncta to various $Ca_V$ channels following stimulation with 40 or 90K, Nim. n ≥ 10 puncta per condition. Pooled data from experiments illustrated in (D) (left bar), in (F) (middle bar), and in Figure S3C (right bar).

(G) Neurons stimulated with 90K, Nim were stained with antibodies against $Ca_V1.3$ and βCaMKII.

Scale bars, 10 μm. Error bars represent SEM.

nearest $Ca_V2.1$ cluster averaged 1.40 ± 0.22 μm (Figure 3F), which is ~10× greater than that found for $Ca_V1.3$ channels ($p < 10^{-5}$) and is large enough to render the signaling susceptible to interception by EGTA (Figures 3A and 3C). Consistent with βCaMKII immunoreactivity, GFP-labeled βCaMKII also translocated to $Ca_V1.3$ puncta upon mild stimulation, but not to $Ca_V2.1$ (Figure S3B). Finally, even selective $Ca_V2$ signaling mobilized βCaMKII puncta to $Ca_V1.3$-associated clusters, not to $Ca_V2.1$ puncta (Figure 3G); nearest-neighbor distances between βCaMKII puncta and $Ca_V1.3$ clusters averaged 0.29 ± 0.07 μm (Figure 3F), similar to the separation observed when $Ca_V1$ channels were the $Ca^{2+}$ source. Thus, βCaMKII was recruited to $Ca_V1$ channel clusters, regardless of the source of $Ca^{2+}$ influx that triggered the aggregation.

The selective aggregation of βCaMKII to sites near $Ca_V1$ channels might involve association of βCaMKII with a scaffolding protein that binds $Ca_V1$, but not $Ca_V2$. Such a scenario has precedence in the hippocampus, in which Densin-180 binds both αCaMKII (Strack et al., 2000; Walikonis et al., 2001) and $Ca_V1.3$ channels (Jenkins et al., 2010). Importantly, the differences in signaling mechanisms employed by $Ca_V1$ and $Ca_V2$ channels in SCGs generalize to CREB signaling in hippocampal neurons; $Ca_V1$ channels mediated signaling to CREB in response to mild depolarization (Figure S4A), and $Ca_V2$ channels were recruited with stronger depolarizations (Figure S4B). Knockdown of Densin-180 (mRNA levels decreased by ~70%; Figure S4C) inhibited depolarization-induced CREB phosphorylation ($p < 0.004$; Figure S4D). Although Densin-180 mRNA is not expressed in SCG neurons, we found Densin-180-like immunoreactivity colocalized with βCaMKII (Figure S4E), suggesting that a relative of Densin-180 may serve the same role.

## Mitochondria Curb Cytosolic $Ca^{2+}$ Transients Arising from $Ca_V2$ Channels

Because $Ca^{2+}$ entering through $Ca_V2$ channels acts on a "distant" $Ca^{2+}$ sensor, we asked whether signaling by $Ca_V2$ was particularly sensitive to spatial attenuation by cytosolic $Ca^{2+}$ buffering. Depolarization-induced $[Ca^{2+}]_i$ rises are strongly attenuated by $Ca^{2+}$ uptake into mitochondria (Babcock and Hille, 1998; Friel and Tsien, 1994; Thayer and Miller, 1990), which grows more pronounced with stronger depolarizations (Friel and Tsien, 1994) that increasingly recruit $Ca_V2$ channels. Accordingly, we tested whether mitochondria preferentially buffer $Ca^{2+}$ entering through $Ca_V2$ channels. To assay mitochondrial buffering, we elicited cytosolic $Ca^{2+}$ transients in depolarized neurons in the absence and then in the presence of carbonyl cyanide p-trifluoromethoxyphenylhydrazone (FCCP), a proton ionophore that greatly reduces the driving force for mitochondrial $Ca^{2+}$ uptake (Figure 4A). During a range of depolarizations, the proportion of the $[Ca^{2+}]_i$ rise buffered by mitochondria was positively correlated with the fraction of total $Ca^{2+}$ current contributed by $Ca_V2$ channels (Figure 4B), but not $Ca_V1$ channels.

Next, we assayed $Ca^{2+}$ uptake into mitochondria by monitoring a hallmark $[Ca^{2+}]_i$ signal, a hump or plateau in the aftermath of mitochondrial $Ca^{2+}$ uptake that reflects restorative extrusion (Babcock and Hille, 1998; Friel and Tsien, 1994; Thayer and Miller, 1990). The plateau was not evident when neurons were stimulated with 20K or 40K, but it grew larger and longer with stronger stimulations (60K and 90K), which recruit large $Ca_V2$ channel fluxes (Figure 4C). $Ca_V2$ blockers largely eliminated the poststimulation plateau after strong depolarization

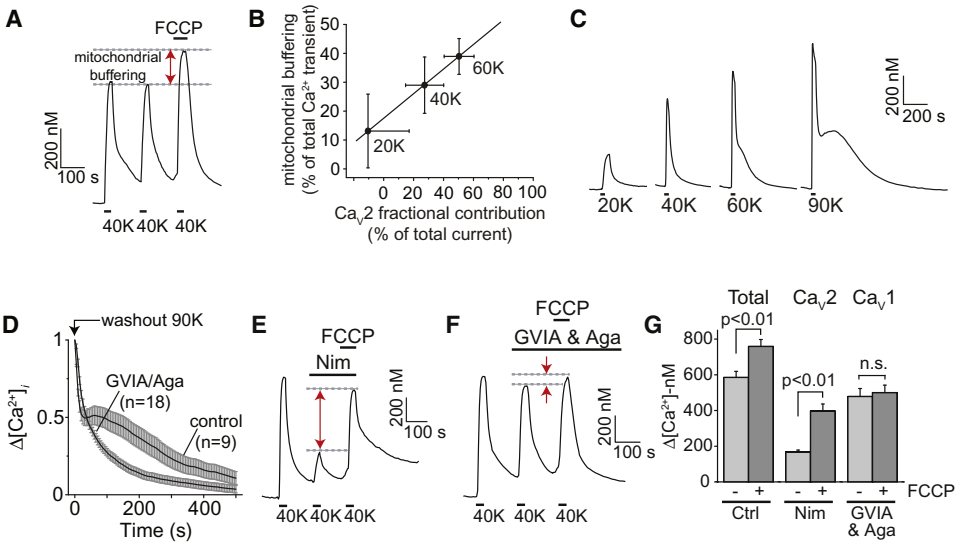


**Figure 4. Mitochondria Preferentially Curb $Ca_V2$-Mediated $Ca^{2+}$ Rises**

(A) Exemplar Fura-2 $Ca^{2+}$ measurement. FCCP (1 μM) potentiated the $Ca^{2+}$ response to 40K, indicating suppression of the peak response by mitochondrial buffering (↔).

(B) Mitochondrial buffering for 20, 40, or 60K, determined as in (A), plotted against the proportion of the current mediated by $Ca_V2$ channels at voltages enforced by $K^+$ challenges (interpolated from data in Figure 2B). Solid line, linear fit (r = 0.99997); n = 18–21 cells.

(C) Exemplar Fura-2 traces induced by $K^+$ depolarizations.

(D) The decay of $[Ca^{2+}]_i$ immediately following 90K stimulation and modification by GVIA/Aga. Data normalized to peak response, with start of wash as 0 s. The traces show mean ±SEM of neurons from ≥4 experiments.

(E and F) Exemplar Fura-2 $Ca^{2+}$ transients measured in response to 40K, showing effects of FCCP in Nim (E) or after preincubation in GVIA/Aga (F).

(G) Summary of peak $[Ca^{2+}]_i$ elevation, measured as in (E) or (F). n ≥ 19 cells from 2–3 platings.

Error bars represent SEM.

(Figure 4D) but spared the peak $Ca^{2+}$ rise ($p > 0.9$), likely limited by intracellular $Ca^{2+}$ buffering mechanisms activating abruptly beyond a critical $Ca^{2+}$ level (Colegrove et al., 2000a, 2000b; Herrington et al., 1996). Finally, we isolated $Ca_V1$- and $Ca_V2$-mediated $[Ca^{2+}]_i$ rises to find out whether they were differently affected by FCCP. Blocking $Ca_V1$ channels removed the majority of the $Ca^{2+}$ rise (Figures 4E and 4G), and the remaining $Ca_V2$-mediated $Ca^{2+}$ transient more than doubled upon the blocking of mitochondrial buffering. In contrast, the much larger $Ca_V1$-mediated $Ca^{2+}$ transient, isolated by blocking $Ca_V2$ channels, was minimally affected by blocking mitochondrial buffering (Figures 4F and 4G). The FCCP effect was related to the *pathway* rather than the *magnitude* of $Ca^{2+}$ influx. Thus, mitochondria appear to act preferentially to help intercept $Ca^{2+}$ entering through $Ca_V2$ rather than $Ca_V1$ channels.

## Measuring Intramitochondrial $Ca^{2+}$ Quantifies Selectivity for $Ca_V2$-Mediated $Ca^{2+}$ Entry

To monitor mitochondrial $Ca^{2+}$ directly, we expressed pericamMT, a ratiometric $Ca^{2+}$ probe that localizes to mitochondria (Nagai et al., 2001). The pericamMT fluorescence ratio increased sharply upon depolarization, reflecting a rapid rise in mitochondrial $Ca^{2+}$ (Figures 5A and 5B). Graded increases in depolarization with 20K, 40K, 60K, and 90K led to progressively larger rises in the pericamMT signal (Figure S5A). Even under conditions in which $Ca_V2$ channels are minority contributors to the $[Ca^{2+}]_i$ rise, $Ca_V2$ blockers prevented the vast majority of the mitochondrial $Ca^{2+}$ rise, which is consistent with the idea that mitochondria preferentially buffer $Ca^{2+}$ from $Ca_V2$ channels. To test this with equally large $[Ca^{2+}]_i$ rises, we compared the effects of 60K depolarization (equal fluxes through $Ca_V1$ and $Ca_V2$ channels; Figures 2B and 2C) with the outcome of depolarization with 20K plus FPL64176, a $Ca_V1$-selective agonist. The $Ca^{2+}$ response to 60K (673.6 ± 62.7 nM) was virtually identical to that produced by 20K with 10 μM FPL (673.8 ± 62.9 nM) (Figure 5C). Under these conditions, the intramitochondrial $Ca^{2+}$ rise was ~3-fold greater when $Ca_V2$ channels contributed to the $Ca^{2+}$ flux (Figure 5D), directly verifying that mitochondria take up $Ca^{2+}$ entering through $Ca_V2$ channels in preference to $Ca^{2+}$ emanating from $Ca_V1$.

## Mitochondria Dampen $Ca_V2$ Signaling to CREB Phosphorylation and Gene Expression

Given that $Ca^{2+}$ acts >1 μm from $Ca_V2$ channels (Figures 3A and 3C), we tested whether eliminating mitochondrial buffering disinhibits $Ca_V2$ signaling to CREB. Though the small $Ca_V2$-mediated $Ca^{2+}$ rise resulting from mild stimulation was insufficient to signal to CREB (Figure 5E), $Ca_V2$ signaling to CREB was unmasked when mitochondrial uptake was blocked (Figures 5E and 5F). The same intervention increased the cytosolic $[Ca^{2+}]_i$ rise more than 2-fold (Figures 4E and 4G). The altered values of $[Ca^{2+}]_i$ and CREB signaling strength in FCCP (Figure 2G, green symbol) fell close to the functional relationship between these two variables that was previously defined for $Ca_V2$ channels.

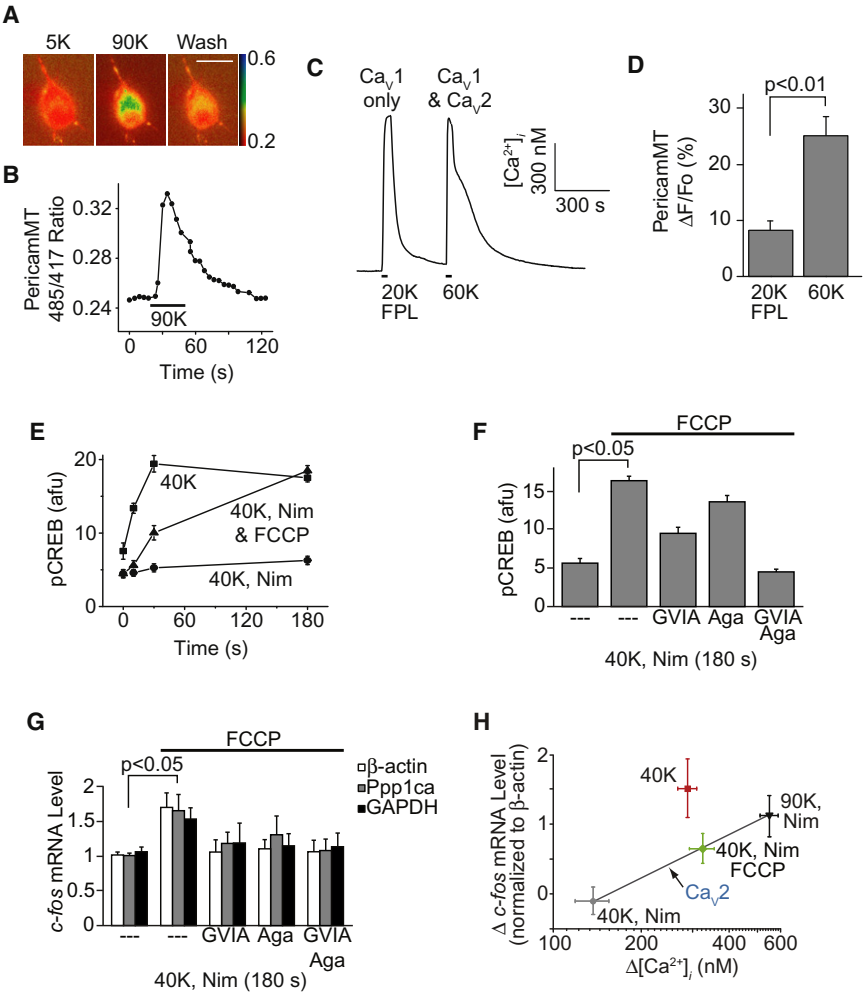


**Figure 5. $Ca^{2+}$ Entering through $Ca_V2$ Channels Is Preferentially Taken Up by Mitochondria**

(A) Exemplar images of a neuron expressing pericamMT. The color scale represents the ratio of emitted fluorescence upon 485 and 417 nm excitation. Scale bar, 25 μm.

(B) Time course of the 485/417 ratio for the same neuron.

(C) Representative Fura-2 trace measuring cytosolic $Ca^{2+}$ levels upon treatment with 20K with FPL64176 (10 μM) or 60K without FPL.

(D) Pooled pericamMT responses from neurons stimulated as in (C), n = 31 (left) or 35 (right) neurons, three platings.

(E) Neurons stimulated with 40K, alone or in the presence of Nim ± FCCP. pCREB immunoreactivity plotted against stimulation duration. n ≥ 38 from three platings.

(F) GVIA/Aga preincubation prevents FCCP-dependent signaling to CREB. n ≥ 33 neurons per condition from two platings.

(G) Neurons stimulated for 3 min as shown, then placed in $5K^+$ Tyrode's for another 42 min before RNA extraction and quantitative RT-PCR for *c-fos*. n = 3–4 experiments done in triplicate.

(H) *c-fos* mRNA levels plotted against the corresponding $[Ca^{2+}]_i$ transient. Fura-2 $Ca^{2+}$ measurements from 25–42 cells from 2–4 independent cultures.

Error bars represent SEM.

FCCP had no effect either in the absence of depolarization or on the $Ca_V1$-mediated pCREB response (data not shown). Confirming that the FCCP effect resulted from $Ca_V2$ channel activity, blocking $Ca_V2$ channels with GVIA and Aga decreased the pCREB responses ($p < 5 \times 10^{-11}$ and $p < 0.01$, respectively) (Figure 5F). These results indicate that mitochondria attenuate the ability of $Ca_V2$ channels to trigger phosphorylation of CREB by limiting $Ca_V2$-mediated $Ca^{2+}$ rises.

To examine whether mitochondrial buffering led to the restriction of $Ca_V2$-mediated induction of pCREB in central nervous system (CNS) neurons, we depolarized hippocampal neurons with 40K in the presence of Nim to prevent $Ca_V1$ signaling and FCCP to block mitochondrial buffering. These conditions triggered CREB phosphorylation mediated by $Ca_V2$ channels (Figure S5B). In additional experiments, we found that mitochondria also appear to curb the ability of $Ca_V2$ channels to drive formation of pCaMKII puncta (Figure S5C), consistent with the involvement of CaMKII as an intermediary in the signaling to pCREB.

Next, we tested whether mitochondrial buffering restricted $Ca_V2$-mediated gene expression. We isolated $Ca_V2$ channels pharmacologically, mildly depolarized neurons for 3 min, and then measured *c-fos* mRNA 42 min later. As with pCREB, the small $Ca_V2$-mediated $Ca^{2+}$ transient did not alter *c-fos* expression relative to controls (data not shown). Importantly, relief of mitochondrial buffering resulted in a $Ca_V2$-mediated increase in *c-fos* mRNA (Figure 5G). Like the pCREB response to FCCP (Figure 2G, green), the $Ca_V2$-mediated gene expression response that was revealed by blocking mitochondrial buffering (Figure 5H, green) fell close to the line defined by the other $Ca_V2$ responses (black and gray symbols); thus, blockade of mitochondrial $Ca^{2+}$ uptake spared the basic relationship between bulk $Ca^{2+}$ rise and response. In contrast, the $Ca_V1$-dependent responses (red symbols) fell significantly above the monotonic relationship defined by $Ca_V2$-dependent responses, which is in keeping with the privileged role of $Ca_V1$ channels.

## Mitochondrial Buffering of $Ca_V2$ Channels Sculpts Spike-Driven CREB Signaling

To relate these principles to physiological activity, we triggered action potentials over a wide range of frequencies, achieving spike rates of up to 100 Hz in direct recordings (insets, Figure 6A). We found that pCREB responses showed a striking bell-shaped dependence on stimulus frequency, with 10 Hz being the most effective frequency, as seen with stimulus trains lasting either 10 or 60 s. Likewise, *c-fos* mRNA levels were increased by 10 Hz, but not 100 Hz, stimulation (Figure 6B).

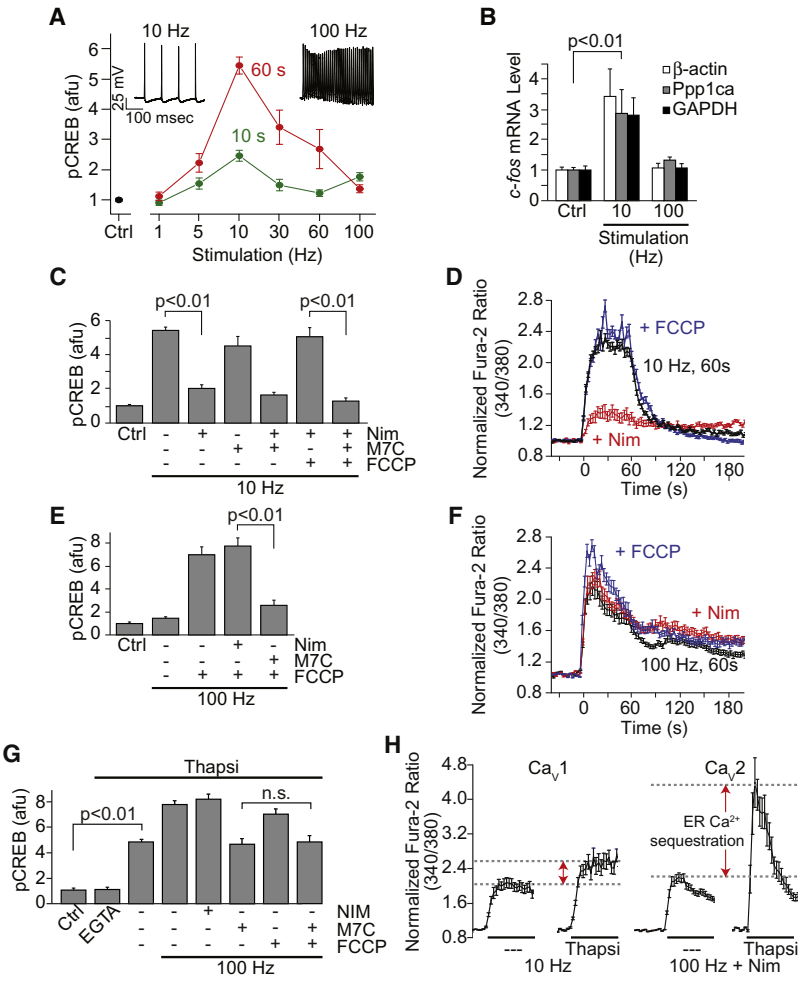


**Figure 6. Mitochondrial Buffering of $Ca_V2$ Channels Sculpts Signaling to CREB Triggered by Action Potentials**

(A) Driving action potentials in SCG neurons with field stimulation (inset: representative current-clamp recordings) revealed a bell-shaped frequency dependence of the pCREB response with a peak at 10 Hz. Data from ≥20 cells per condition from two platings.

(B) *c-fos* mRNA levels, measured after 180 s stimulation followed by 42 min rest. n = 9 coverslips from three platings.

(C–F) (C and E) CREB phosphorylation measured following stimulation at 10 Hz (C) or 100 Hz (E). Stimulation for 60 s, with and without Nim, M7C (5 μM), and FCCP. ≥20 cells per condition from two platings. (D and F) Fura-2 $Ca^{2+}$ transients, recorded with 10 or 100 Hz stimulation, normalized to basal ratiometric level and pooled. Data from ≥30 cells per condition, two platings.

(G) CREB phosphorylation after field stimulation with Thapsi (2 μM), ±EGTA. Neurons were preincubated for 1 min with Thapsi or FCCP, ±Nim or M7C, before 100 Hz stimulation. ≥20 cells per condition from two platings.

(H) Effects of Thapsi on Fura-2 $Ca^{2+}$ responses to stimulation at 10 Hz or at 100 Hz with Nim present. ≥30 cells from two platings.

Error bars represent SEM.

Does the superior efficacy of 10 Hz firing relate to the potency of $Ca_V1$ versus $Ca_V2$ signaling? The 10 Hz-induced increases in pCREB levels were largely abolished by the $Ca_V1$ blocker Nim, but not by ω-conotoxin MVIIC (M7C), a generic blocker of $Ca_V2.1$ and $Ca_V2.2$ (Figure 6C); these treatments did not affect field stimulation-triggered spiking. As with 40K stimulation, 10 Hz stimulation in the presence of Nim and FCCP unmasked the role of mitochondrial $Ca^{2+}$ uptake in $Ca_V2$ signaling to CREB (Figure 6C). Further, bulk $Ca^{2+}$ rises evoked by 10 Hz stimulation were largely inhibited by Nim and only marginally augmented by FCCP (~17%) (Figure 6D). In contrast, the 100 Hz-induced $Ca^{2+}$ rise was comparable in size to the 10 Hz response but was unaffected by Nim (Figures 6D and 6F), indicating that the $Ca^{2+}$ rise arose from $Ca_V2$ channels. The exclusively $Ca_V2$-mediated $Ca^{2+}$ influx would put communication to CREB at a strong disadvantage due in part to mitochondrial $Ca^{2+}$ uptake. Indeed, a sizeable pCREB response to 100 Hz stimulation was unmasked by FCCP (Figure 6E). This response was unaffected by Nim but largely abolished by blocking $Ca_V2$ channels. Thus, the falling phase of the bell-shaped rate dependence (Figure 6A) arises from a declining contribution from $Ca_V1$ channels and a weakness of $Ca_V2$ channels in activating CREB signaling due to mitochondrial buffering, indicating a physiological role for mitochondria in shaping the response to action potentials.

## ER $Ca^{2+}$ Uptake Discriminates between $Ca_V1$- and $Ca_V2$-Mediated $Ca^{2+}$ Entry

How is $Ca_V2$-mediated $Ca^{2+}$ entry preferentially linked to mitochondrial $Ca^{2+}$ uptake? The spatial separation between $Ca_V1$ and $Ca_V2$ channels, the former colocalized with βCaMKII puncta and the latter not, might allow the channels to be differentially apposed to intracellular $Ca^{2+}$ stores. We found no overt spatial link between $Ca_V2$ channels and mitochondria. This lack of $Ca_V2$-mitochondria apposition may be explained by data from frog sympathetic neurons showing that mitochondria are separated from the cell surface by a peripheral ring of ER (McDonough et al., 2000). Because mitochondria can couple to the ER (Montero et al., 2000; Rizzuto et al., 1993), $Ca^{2+}$ channel-type specificity of mitochondrial $Ca^{2+}$ sequestration may arise secondarily from $Ca_V2$ coupling to ER.

If sarco(endo)plasmic reticulum $Ca^{2+}$ ATPase (SERCA) pumps were positioned just beneath the plasma membrane, blockade with thapsigargin (Thapsi) may trigger subsurface $Ca^{2+}$ signaling similar to that evoked by $Ca^{2+}$ entry via $Ca_V2$ channels. Depleting ER $Ca^{2+}$ with Thapsi (indicated by formation of puncta of the ER $Ca^{2+}$ sensor protein STIM1; data not shown) strongly elevated pCREB in an EGTA-dependent manner (Figure 6G). Thapsi also greatly increased the weight of βCaMKII puncta (data not shown). In contrast, FCCP alone neither increased CaMKII activation (Figure 6) nor elevated basal pCREB (data not shown).

If the peripheral ER normally passes $Ca^{2+}$ through to mitochondria in response to depolarization, blockade of ER $Ca^{2+}$

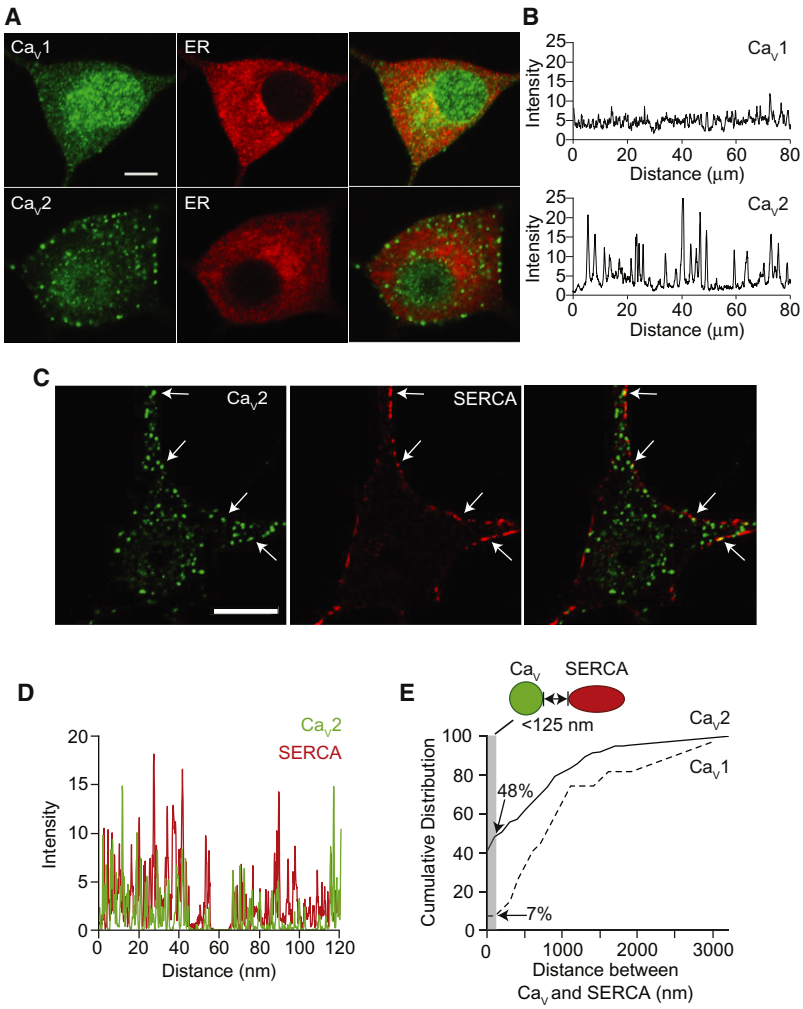


**Figure 7. Factors Supporting ER Preference for $Ca_V2$-Derived $Ca^{2+}$**

(A) Exemplar confocal images of cultured SCG neurons immunostained with antibodies directed against either $Ca_V1.3$ or $Ca_V2.1$ and the ER marker PDI. Scale bar, 10 μm.

(B) Intensity profiles extracted from images in (A). Respective profiles scaled to have equal areas.

(C) Exemplar confocal image of an SCG neuron immunostained with antibodies directed against $Ca_V2.1$ and SERCA. Scale bar, 10 μm.

(D) Intensity profile extracted from images in (C).

(E) Cumulative distribution of edge-to-edge distances between $Ca_V1.3$ or $Ca_V2.1$ puncta and the closest SERCA punctum. In 48% of cases, the SERCA punctum frankly overlapped with the profile of the $Ca_V2.1$ puncta, extended by 125 nm to allow for lateral diffusion of $Ca^{2+}$.

uptake should mimic and largely occlude the effects of inhibiting mitochondrial $Ca^{2+}$ uptake. Indeed, Thapsi caused a >2-fold increase in the 100 Hz-evoked peak $[Ca^{2+}]_i$ (Figure 6H, right), as great as that produced by FCCP + Thapsi (Figure S6A). This near equivalency would be expected if the mitochondrial $Ca^{2+}$ uniporter lost effectiveness in the absence of ER-mediated, local $Ca^{2+}$ elevation in a restricted ER-mitochondrial space (Kirichok et al., 2004; Montero et al., 2000; Rizzuto et al., 1993). In contrast, FCCP without Thapsi produced only a modest increase in peak $[Ca^{2+}]_i$ (~25%) (Figure S6B), as though the loss of mitochondrial $Ca^{2+}$ uptake spared the ability of ER to sequester $Ca^{2+}$. The pCREB response was elevated to the same level by Thapsi alone as by Thapsi with FCCP (fourth and seventh bars, Figure 6G), which was expected from their combined effect on $Ca^{2+}$ rises. Confirming $Ca_V2$ involvement, the pCREB signal was inhibited by M7C (Figure 6G).

By comparing the effects of ER buffering on $Ca_V1$ and $Ca_V2$ channels, we found that Thapsi increased the $Ca_V2$-mediated $Ca^{2+}$ transient in response to 100 Hz by >2-fold but only augmented the largely $Ca_V1$ response to 10 Hz by ~26% (Figure 6H). This shows that ER preferentially couples to $Ca_V2$ over $Ca_V1$ channels, duplicating the pattern that we found for mitochondrial $Ca^{2+}$ uptake with FCCP (Figures 4E and 4F).

Having established a functional link between $Ca_V2$ channels and ER, we examined the distribution of $Ca_V1$ and $Ca_V2$ channels relative to the ER. Immunostained $Ca_V2$ channels were found in large clusters, whereas $Ca_V1$ channels were more diffusely distributed with smaller and less intense puncta (Figures 7A and 7B). However, neither channel type was particularly colocalized with a luminal ER marker, disulphide isomerase (PDI) (Figure 7A). If not $Ca_V2$ localization to ER in general, what about apposition to the sites of $Ca^{2+}$ uptake, the SERCA pumps? Mindful that $Ca_V$ channels produce a plume of high $[Ca^{2+}]$ that reaches hundreds of micromolar below a channel cluster but falls off over distances of ~100 nm outside of it (Roberts, 1994), we estimated distances between $Ca_V2.1$ puncta and immunostained SERCA pumps in confocal images (Figure 7C). Analysis of intensity profiles along the edge of the cell indicated that $Ca_V2$ clusters often coincided with regions of SERCA pump staining (Figure 7D). Nearly half (48%) of $Ca_V2$ puncta overlapped with or were within <125 nm of SERCA pumps. Conversely, only 7% of $Ca_V1$ puncta fit this criterion (Figure 7E). Therefore, SERCA pumps are much less likely to encounter $Ca^{2+}$ plumes emanating from $Ca_V1$ channel clusters. The largeness of $Ca_V2$ channel clusters will also greatly favor SERCA uptake of $Ca_V2$-derived $Ca^{2+}$ because SERCA transport is a sigmoid function of $[Ca^{2+}]_i$ (Inesi et al., 1990; Satoh et al., 2011).

## DISCUSSION

### Multiple Factors Engender Differential Abilities to $Ca_V1$ and $Ca_V2$ Channels for Signaling to the Nucleus

Coupling between membrane depolarization and gene expression is critical for long-term changes in neural function, yet much remains unknown about how $Ca^{2+}$ channels activate nuclear transcription factors. We found that two major classes

of $Ca^{2+}$ channels, $Ca_V1$ (L-type) and $Ca_V2$ (N- and P/Q-type), support excitation-pCREB coupling with voltage dependence comparably steep to E-C coupling and E-S coupling. $Ca_V2$ channels signal to pCREB with ~70-fold lower strength than $Ca_V1$ channels with the same depolarization. We traced this difference in potency to multiple factors. First, $Ca_V1$ channels activate at more negative potentials, giving them an intrinsic gating advantage. Second, $Ca_V1$ channels are endowed with nanodomain access to local biochemical mechanisms involving CaMKII, whereas $Ca_V2$ channels must communicate via $Ca^{2+}$ elevations over a greater distance (>1 μm). Third, ER and mitochondria preferentially buffer $Ca^{2+}$ entering through $Ca_V2$ channels. Collectively, these factors allow $Ca_V1$ channels to outweigh $Ca_V2$ channels in activity-dependent signaling to the nucleus.

## Coexistence of Nanodomain and Supramicron $Ca^{2+}$ Signaling Mechanisms

Beyond differences in channel gating, our expectation was that CREB phosphorylation would be simply related to the bulk $Ca^{2+}$ rise, irrespective of $Ca^{2+}$ source. This would be true if $Ca^{2+}$ entry worked *solely* by raising nuclear $[Ca^{2+}]_i$, which is nearly the same as bulk somatic $[Ca^{2+}]_i$ (Eder and Bading, 2007). To the contrary, we found that $Ca_V1$ and $Ca_V2$ channels work along different operating curves ~10-fold apart. Thus, over and above differences in channel gating, $Ca^{2+}$ rises generated by $Ca_V1$ channels are far more efficacious than those arising from $Ca_V2$ channels.

The difference in efficacy stems from sharp differences in how the two classes of $Ca^{2+}$ channels employ $Ca^{2+}$ signaling. $Ca^{2+}$ entering through $Ca_V1$ channels acts locally in a nanodomain at the channel mouth (Wheeler et al., 2008). The quantitative advantage of $Ca_V1$ over $Ca_V2$ channels implies that the $Ca^{2+}$ sensor experiences a local $[Ca^{2+}]_i$ ~10-fold higher than bulk $[Ca^{2+}]_i$. This can easily be attained <40 nm from the $Ca_V1$ pore mouth (Neher, 1986; Roberts, 1993) in a domain containing millimolar CaM (Mori et al., 2004), along with tethered CaMKII (Grueter et al., 2006; Hudmon et al., 2005) and newly recruited CaMKII (Wheeler et al., 2008) as targets.

Like $Ca_V1$ channels, $Ca_V2$ channels drive formation of pCaMKII puncta and signal to pCREB and gene transcription. The key difference is that $Ca^{2+}$ entering through $Ca_V2$ channels acts at a sufficient distance to be intercepted by EGTA and thus requires larger $Ca_V2$ fluxes to achieve similar $[Ca^{2+}]$ at the site of action. From our data, we conclude that $Ca_V2$ channels communicate on a supramicron scale, presumably engaging the same signaling sites employed by $Ca_V1$ channels, and that mobilization of βCaMKII is driven by diffusion and binding to $Ca_V1$-proximal kinase-binding sites, not by homing toward the $Ca^{2+}$ source.

## Mitochondria Preferentially Sequester $Ca_V2$-Mediated $Ca^{2+}$ Influx

Our data support an unexpected role for mitochondria in the preferential uptake of $Ca^{2+}$ entering via $Ca_v2$ channels, adding to the well-established role of mitochondria in shaping neuronal $Ca^{2+}$ transients (Alonso et al., 2009; Babcock and Hille, 1998; Friel, 2000). First, the fraction of the $Ca^{2+}$ transient buffered by mitochondria scaled with the contribution of $Ca_V2$ to the total transient. Second, blocking $Ca_V2$ channels largely eliminated a hallmark of mitochondrial $Ca^{2+}$ uptake, the plateau in the $Ca^{2+}$ decay phase. Third, suppression of mitochondrial $Ca^{2+}$ uptake with FCCP greatly potentiated bulk $[Ca^{2+}]_i$ rises mediated by $Ca_V2$, but not $Ca_V1$. Fourth, a mitochondrial $Ca^{2+}$ sensor responded much more strongly to $Ca_V2$ than $Ca_V1$ channels.

The $Ca_V2$-mitochondria interaction may also tie metabolism to $Ca_V2$ activity, which should modulate intramitochondrial dehydrogenases (McCormack et al., 1990) in what could be termed excitation-metabolism coupling. $Ca^{2+}$ uptake into mitochondria can also have dire consequences under pathophysiological conditions (Hajnóczky et al., 2006; Nicholls and Budd, 2000). The $Ca_V2.2$-selective pain drug Prialt is strongly neuroprotective under postischemic conditions (Twede et al., 2009; Valentino et al., 1993; Yenari et al., 1996), hinting that tight functional coupling of $Ca_V2$ channels to mitochondria might exacerbate cell death after head injury or stroke.

## Preference of SERCA Pumps for $Ca_V2$-Derived $Ca^{2+}$

Our data suggest that the preference for $Ca^{2+}$ entry mediated by $Ca_V2$ likely arises from their close relationship with SERCA pumps in subsurface ER. We found that: (1) SERCA pump blockade produced EGTA-sensitive CREB phosphorylation, just like $Ca_V2$ channels; (2) the ER much more efficiently sequestered $Ca^{2+}$ from $Ca_V2$ than from $Ca_V1$; and (3) blockade of ER $Ca^{2+}$ uptake mimics and occludes the effect of inhibiting mitochondrial $Ca^{2+}$ uptake. Our results dovetail with previous findings that: (1) $Ca_V2.2$ channels in the surface membrane appose the ER, coming within tens of nanometers of ryanodine receptor (RyR) channels (Akita and Kuba, 2000); (2) mitochondria form an annulus just central to the most peripheral ring of ER (McDonough et al., 2000); and (3) in electron micrographs, mitochondria sometimes flatten up against the nuclear-facing aspect of subsurface ER cisterns (Henkart et al., 1976). These structural arrangements favor an efficient serial transfer of $Ca^{2+}$ from $Ca^{2+}$ channels to peripheral ER to mitochondria.

In conclusion, our study uncovers fundamental differences in the way that $Ca^{2+}$ ions entering the cell through $Ca_V1$ versus $Ca_V2$ channels activate transcription. $Ca_V1$-derived $Ca^{2+}$ acts locally, interacting with signaling machinery in the immediate vicinity of the channel to couple membrane depolarization to gene expression. In contrast, high-density $Ca_V2$ channel clusters generate large local elevations of $[Ca^{2+}]_i$ in proximity to SERCA pumps, leading to preferential uptake by ER and mitochondria. Although this might underlie an unexpected mode of excitation-metabolism coupling, it strongly dampens $Ca_V2$ engagement of E-T coupling.

## EXPERIMENTAL PROCEDURES

Additional information regarding plasmids, buffers, antibodies, primer sequences, and detailed procedures are described in Supplemental Information.

### Primary Cultures of SCG and Hippocampal Neurons

SCG neurons and hippocampal pyramidal neurons were cultured as previously described (Groth et al., 2011; Wheeler et al., 2008), with minor modifications (see Supplemental Information).

### Drug Treatments and Stimulation

To induce CREB phosphorylation, we stimulated SCG or hippocampal neurons with the indicated K solution at room temperature for 2.5–180 s, followed by 45 s in control (5K) Tyrode's solution before fixation (see Wheeler et al., 2008).

### Electrophysiology

Whole-cell voltage-clamp recordings were performed as previously described (Wheeler et al., 2008). Toxins were added directly to the bath; the toxins were considered to have achieved maximum effect after the currents became stable.

### Field Stimulation

We stimulated SCG neurons with 3 ms square wave pulses in Tyrode's solution by using two platinum electrodes a distance of ~10 mm apart. A Grass S11 stimulator controlled pulse amplitude and duration. The stimulus amplitudes were set to 20% above threshold. We perfused bath solution at ~0.2 ml/min to prevent toxicity due to hydrolysis.

### Cytosolic $Ca^{2+}$ Imaging

We loaded SCG neurons in conditioned medium for 30–60 min with 2 μM Fura-2 AM (Invitrogen) and 0.02% Pluronic F-127 (Invitrogen) in a 37°C/5% $CO_2$ incubator as described previously (see Wheeler et al., 2008).

### PericamMT Imaging

We imaged lentivirus-infected SCG neurons expressing PericamMT on days in vitro (DIV) 4–5, sampling every 3 s by excitation at 485 and 417 nm; emission was detected at 535 nm. We background subtracted regions of interest (ROIs) that excluded the neuron's nucleus and determined the 485/417 ratio. We blocked $Ca_V2$ channels as in pCREB experiments.

### Real-Time PCR

Following stimulation, we placed coverslips in RNALater (QIAGEN) at 4°C. We isolated total RNA by using the RNeasy Micro kit (QIAGEN) and reverse transcribed into cDNA by using a QuantiTect real-time PCR (RT-PCR) kit (QIAGEN). Each sample was from one 10 mm coverslip. Real-time qPCR was performed in an Opticon 2 RT-PCR machine (Bio-Rad) by using SYBR-green PCR master mix (Fermentas). In each experiment, three separate coverslips were used per condition, and each cDNA sample was run in duplicate. We normalized specific target mRNA levels to three of four different housekeeping genes: β-actin, RPL19 or Ppp1ca, and GAPDH.

## SUPPLEMENTAL INFORMATION

Supplemental Information includes Extended Experimental Procedures and six figures and can be found with this article online at doi:10.1016/j.cell.2012.03.041.

## ACKNOWLEDGMENTS

We thank Rich Lewis, David Friel, Michael Tadross, Damon Poburko, Yulong Li, Hyokeun Park, Haruhiko Bito, S. Brian Andrews, Paul De Koninck, and George Miljanich for helpful discussions and Atsushi Miyawaki for PericamMT. This work was supported by research grants to R.W.T. from NIGMS, NINDS, and the Mathers Foundation. S.F.O. is supported by the Burnett Family Foundation and an NRSA from the NIMH (F31MH084430).

Received: June 12, 2009
Revised: November 11, 2011
Accepted: March 7, 2012
Published: May 24, 2012

## REFERENCES

Adams, J.P., and Dudek, S.M. (2005). Late-phase long-term potentiation: getting to the nucleus. Nat. Rev. Neurosci. *6*, 737–743.

Akita, T., and Kuba, K. (2000). Functional triads consisting of ryanodine receptors, $Ca(^{2+})$ channels, and $Ca(^{2+})$-activated $K(^{+})$ channels in bullfrog sympathetic neurons. Plastic modulation of action potential. J. Gen. Physiol. *116*, 697–720.

Alonso, M.T., Manjarrés, I.M., and García-Sancho, J. (2009). Modulation of calcium signalling by intracellular organelles seen with targeted aequorins. Acta Physiol. (Oxf.) *195*, 37–49.

Babcock, D.F., and Hille, B. (1998). Mitochondrial oversight of cellular $Ca^{2+}$ signaling. Curr. Opin. Neurobiol. *8*, 398–404.

Berridge, M.J. (2008). Smooth muscle cell calcium activation mechanisms. J. Physiol. *586*, 5047–5061.

Brosenitsch, T.A., and Katz, D.M. (2001). Physiological patterns of electrical stimulation can induce neuronal gene expression by activating N-type calcium channels. J. Neurosci. *21*, 2571–2579.

Catterall, W.A. (2000). Structure and regulation of voltage-gated $Ca2^{+}$ channels. Annu. Rev. Cell Dev. Biol. *16*, 521–555.

Colegrove, S.L., Albrecht, M.A., and Friel, D.D. (2000a). Dissection of mitochondrial $Ca2^{+}$ uptake and release fluxes in situ after depolarization-evoked $[Ca^{2+}]_i$ elevations in sympathetic neurons. J. Gen. Physiol. *115*, 351–370.

Colegrove, S.L., Albrecht, M.A., and Friel, D.D. (2000b). Quantitative analysis of mitochondrial $Ca2^{+}$ uptake and release pathways in sympathetic neurons. Reconstruction of the recovery after depolarization-evoked $[Ca^{2+}]_i$ elevations. J. Gen. Physiol. *115*, 371–388.

Deisseroth, K., Bito, H., and Tsien, R.W. (1996). Signaling from synapse to nucleus: postsynaptic CREB phosphorylation during multiple forms of hippocampal synaptic plasticity. Neuron *16*, 89–101.

Deisseroth, K., Mermelstein, P.G., Xia, H., and Tsien, R.W. (2003). Signaling from synapse to nucleus: the logic behind the mechanisms. Curr. Opin. Neurobiol. *13*, 354–365.

Dolmetsch, R.E., Pajvani, U., Fife, K., Spotts, J.M., and Greenberg, M.E. (2001). Signaling to the nucleus by an L-type calcium channel-calmodulin complex through the MAP kinase pathway. Science *294*, 333–339.

Dolphin, A.C. (2006). A short history of voltage-gated calcium channels. Br. J. Pharmacol. *147* (*Suppl 1*), S56–S62.

Eder, A., and Bading, H. (2007). Calcium signals can freely cross the nuclear envelope in hippocampal neurons: somatic calcium increases generate nuclear calcium transients. BMC Neurosci. *8*, 57.

Flavell, S.W., and Greenberg, M.E. (2008). Signaling mechanisms linking neuronal activity to gene expression and plasticity of the nervous system. Annu. Rev. Neurosci. *31*, 563–590.

Friel, D.D. (2000). Mitochondria as regulators of stimulus-evoked calcium signals in neurons. Cell Calcium *28*, 307–316.

Friel, D.D., and Tsien, R.W. (1994). An FCCP-sensitive $Ca2^{+}$ store in bullfrog sympathetic neurons and its participation in stimulus-evoked changes in $[Ca2^{+}]$i. J. Neurosci. *14*, 4007–4024.

Greenberg, M.E., Ziff, E.B., and Greene, L.A. (1986). Stimulation of neuronal acetylcholine receptors induces rapid gene transcription. Science *234*, 80–83.

Groth, R.D., Lindskog, M., Thiagarajan, T.C., Li, L., and Tsien, R.W. (2011). Beta $Ca2^{+}$/CaM-dependent kinase type II triggers upregulation of GluA1 to coordinate adaptation to synaptic inactivity in hippocampal neurons. Proc. Natl. Acad. Sci. USA *108*, 828–833.

Grueter, C.E., Abiria, S.A., Dzhura, I., Wu, Y., Ham, A.J., Mohler, P.J., Anderson, M.E., and Colbran, R.J. (2006). L-type $Ca2^{+}$ channel facilitation mediated by phosphorylation of the beta subunit by CaMKII. Mol. Cell *23*, 641–650.

Hajnóczky, G., Csordás, G., Das, S., Garcia-Perez, C., Saotome, M., Sinha Roy, S., and Yi, M. (2006). Mitochondrial calcium signalling and cell death: approaches for assessing the role of mitochondrial $Ca2^{+}$ uptake in apoptosis. Cell Calcium *40*, 553–560.

Hardingham, G.E., Chawla, S., Johnson, C.M., and Bading, H. (1997). Distinct functions of nuclear and cytoplasmic calcium in the control of gene expression. Nature *385*, 260–265.

Hardingham, G.E., Arnold, F.J., and Bading, H. (2001). Nuclear calcium signaling controls CREB-mediated gene expression triggered by synaptic activity. Nat. Neurosci. *4*, 261–267.

Henkart, M., Landis, D.M., and Reese, T.S. (1976). Similarity of junctions between plasma membranes and endoplasmic reticulum in muscle and neurons. J. Cell Biol. *70*, 338–347.

Herrington, J., Park, Y.B., Babcock, D.F., and Hille, B. (1996). Dominant role of mitochondria in clearance of large $Ca2^+$ loads from rat adrenal chromaffin cells. Neuron *16*, 219–228.

Hudmon, A., Schulman, H., Kim, J., Maltez, J.M., Tsien, R.W., and Pitt, G.S. (2005). CaMKII tethers to L-type $Ca2^+$ channels, establishing a local and dedicated integrator of $Ca2^+$ signals for facilitation. J. Cell Biol. *171*, 537–547.

Inesi, G., Sumbilla, C., and Kirtley, M.E. (1990). Relationships of molecular structure and function in Ca2(+)-transport ATPase. Physiol. Rev. *70*, 749–760.

Jenkins, M.A., Christel, C.J., Jiao, Y., Abiria, S., Kim, K.Y., Usachev, Y.M., Obermair, G.J., Colbran, R.J., and Lee, A. (2010). $Ca2^+$-dependent facilitation of Cav1.3 $Ca2^+$ channels by densin and $Ca2^+$/calmodulin-dependent protein kinase II. J. Neurosci. *30*, 5125–5135.

Jiang, X., Lautermilch, N.J., Watari, H., Westenbroek, R.E., Scheuer, T., and Catterall, W.A. (2008). Modulation of CaV2.1 channels by $Ca2^+$/calmodulin-dependent protein kinase II bound to the C-terminal domain. Proc. Natl. Acad. Sci. USA *105*, 341–346.

Kasai, H., and Neher, E. (1992). Dihydropyridine-sensitive and omega-conotoxin-sensitive calcium channels in a mammalian neuroblastoma-glioma cell line. J. Physiol. *448*, 161–188.

Kavalali, E.T., Zhuo, M., Bito, H., and Tsien, R.W. (1997). Dendritic $Ca2^+$ channels characterized by recordings from isolated hippocampal dendritic segments. Neuron *18*, 651–663.

Kirichok, Y., Krapivinsky, G., and Clapham, D.E. (2004). The mitochondrial calcium uniporter is a highly selective ion channel. Nature *427*, 360–364.

Liu, Z., Ren, J., and Murphy, T.H. (2003). Decoding of synaptic voltage waveforms by specific classes of recombinant high-threshold $Ca(2^+)$ channels. J. Physiol. *553*, 473–488.

McCormack, J.G., Halestrap, A.P., and Denton, R.M. (1990). Role of calcium ions in regulation of mammalian intramitochondrial metabolism. Physiol. Rev. *70*, 391–425.

McDonough, S.I., Cseresnyés, Z., and Schneider, M.F. (2000). Origin sites of calcium release and calcium oscillations in frog sympathetic neurons. J. Neurosci. *20*, 9059–9070.

Montero, M., Alonso, M.T., Carnicero, E., Cuchillo-Ibáñez, I., Albillos, A., García, A.G., García-Sancho, J., and Alvarez, J. (2000). Chromaffin-cell stimulation triggers fast millimolar mitochondrial $Ca2^+$ transients that modulate secretion. Nat. Cell Biol. *2*, 57–61.

Morgan, J.I., and Curran, T. (1986). Role of ion flux in the control of c-fos expression. Nature *322*, 552–555.

Mori, M.X., Erickson, M.G., and Yue, D.T. (2004). Functional stoichiometry and local enrichment of calmodulin interacting with $Ca^{2+}$ channels. Science *304*, 432–435.

Murphy, T.H., Worley, P.F., and Baraban, J.M. (1991). L-type voltage-sensitive calcium channels mediate synaptic activation of immediate early genes. Neuron *7*, 625–635.

Nagai, T., Sawano, A., Park, E.S., and Miyawaki, A. (2001). Circularly permuted green fluorescent proteins engineered to sense $Ca2^+$. Proc. Natl. Acad. Sci. USA *98*, 3197–3202.

Neher, E. (1986). Concentration profiles of intracellular calcium in the presence of a diffusible chelators. In Calcium Electrogenesis and Neuronal Functioning, U. Heinemann, M. Klee, E. Neher, and W. Singer, eds. (Berlin: Springer-Verlag), pp. 80–96.

Nicholls, D.G., and Budd, S.L. (2000). Mitochondria and neuronal survival. Physiol. Rev. *80*, 315–360.

Oliveria, S.F., Dell'Acqua, M.L., and Sather, W.A. (2007). AKAP79/150 anchoring of calcineurin controls neuronal L-type $Ca2^+$ channel activity and nuclear signaling. Neuron *55*, 261–275.

Randall, A., and Tsien, R.W. (1995). Pharmacological dissection of multiple types of $Ca2^+$ channel currents in rat cerebellar granule neurons. J. Neurosci. *15*, 2995–3012.

Regan, L.J., Sah, D.W., and Bean, B.P. (1991). $Ca2^+$ channels in rat central and peripheral neurons: high-threshold current resistant to dihydropyridine blockers and omega-conotoxin. Neuron *6*, 269–280.

Rizzuto, R., Brini, M., Murgia, M., and Pozzan, T. (1993). Microdomains with high $Ca^{2+}$ close to IP3-sensitive channels that are sensed by neighboring mitochondria. Science *262*, 744–747.

Roberts, W.M. (1993). Spatial calcium buffering in saccular hair cells. Nature *363*, 74–76.

Roberts, W.M. (1994). Localization of calcium signals by a mobile calcium buffer in frog saccular hair cells. J. Neurosci. *14*, 3246–3262.

Saha, R.N., and Dudek, S.M. (2008). Action potentials: to the nucleus and beyond. Exp. Biol. Med. (Maywood) *233*, 385–393.

Satoh, K., Matsu-Ura, T., Enomoto, M., Nakamura, H., Michikawa, T., and Mikoshiba, K. (2011). Highly cooperative dependence of sarco/endoplasmic reticulum calcium ATPase SERCA2a pump activity on cytosolic calcium in living cells. J. Biol. Chem. *286*, 20591–20599.

Sheng, M., McFadden, G., and Greenberg, M.E. (1990). Membrane depolarization and calcium induce c-fos transcription via phosphorylation of transcription factor CREB. Neuron *4*, 571–582.

Shieh, P.B., Hu, S.C., Bobb, K., Timmusk, T., and Ghosh, A. (1998). Identification of a signaling pathway involved in calcium regulation of BDNF expression. Neuron *20*, 727–740.

Strack, S., Robison, A.J., Bass, M.A., and Colbran, R.J. (2000). Association of calcium/calmodulin-dependent kinase II with developmentally regulated splice variants of the postsynaptic density protein densin-180. J. Biol. Chem. *275*, 25061–25064.

Sudhof, T.C. (2004). The synaptic vesicle cycle. Annu. Rev. Neurosci. *27*, 509–547.

Sutton, K.G., McRory, J.E., Guthrie, H., Murphy, T.H., and Snutch, T.P. (1999). P/Q-type calcium channels mediate the activity-dependent feedback of syntaxin-1A. Nature *401*, 800–804.

Tao, X., Finkbeiner, S., Arnold, D.B., Shaywitz, A.J., and Greenberg, M.E. (1998). $Ca^{2+}$ influx regulates BDNF transcription by a CREB family transcription factor-dependent mechanism. Neuron *20*, 709–726.

Thayer, S.A., and Miller, R.J. (1990). Regulation of the intracellular free calcium concentration in single rat dorsal root ganglion neurones in vitro. J. Physiol. *425*, 85–115.

Tsien, R.W., Ellinor, P.T., and Horne, W.A. (1991). Molecular diversity of voltage-dependent $Ca2^+$ channels. Trends Pharmacol. Sci. *12*, 349–354.

Twede, V.D., Miljanich, G., Olivera, B.M., and Bulaj, G. (2009). Neuroprotective and cardioprotective conopeptides: an emerging class of drug leads. Curr. Opin. Drug Discov. Devel. *12*, 231–239.

Valentino, K., Newcomb, R., Gadbois, T., Singh, T., Bowersox, S., Bitner, S., Justice, A., Yamashiro, D., Hoffman, B.B., Ciaranello, R., et al. (1993). A selective N-type calcium channel antagonist protects against neuronal loss after global cerebral ischemia. Proc. Natl. Acad. Sci. USA *90*, 7894–7897.

Walikonis, R.S., Oguni, A., Khorosheva, E.M., Jeng, C.J., Asuncion, F.J., and Kennedy, M.B. (2001). Densin-180 forms a ternary complex with the (alpha)-subunit of $Ca2^+$/calmodulin-dependent protein kinase II and (alpha)-actinin. J. Neurosci. *21*, 423–433.

Weick, J.P., Groth, R.D., Isaksen, A.L., and Mermelstein, P.G. (2003). Interactions with PDZ proteins are required for L-type calcium channels to activate cAMP response element-binding protein-dependent gene expression. J. Neurosci. *23*, 3446–3456.

Wheeler, D.G., and Cooper, E. (2001). Depolarization strongly induces human cytomegalovirus major immediate-early promoter/enhancer activity in neurons. J. Biol. Chem. *276*, 31978–31985.

Wheeler, D.G., Barrett, C.F., and Tsien, R.W. (2006). L-type calcium channel ligands block nicotine-induced signaling to CREB by inhibiting nicotinic receptors. Neuropharmacology *51*, 27–36.

Wheeler, D.G., Barrett, C.F., Groth, R.D., Safa, P., and Tsien, R.W. (2008). CaMKII locally encodes L-type channel activity to signal to nuclear CREB in excitation-transcription coupling. J. Cell Biol. *183*, 849–863.

Yenari, M.A., Palmer, J.T., Sun, G.H., de Crespigny, A., Mosely, M.E., and Steinberg, G.K. (1996). Time-course and treatment response with SNX-111, an N-type calcium channel blocker, in a rodent model of focal cerebral ischemia using diffusion-weighted MRI. Brain Res. *739*, 36–45.

Zhao, R., Liu, L., and Rittenhouse, A.R. (2007). $Ca2^{+}$ influx through both L- and N-type $Ca2^{+}$ channels increases c-fos expression by electrical stimulation of sympathetic neurons. Eur. J. Neurosci. *25*, 1127–1135.